



## Fabrication and Characterization of Nanocomposites Based on NiFe<sub>2</sub>O<sub>4</sub> Nanoparticles and Epoxy Polymer

Md. Abdus Sabur<sup>1</sup>, G. M. Shafiur Rahman<sup>1</sup>, Md. Kamruzzaman<sup>1</sup>,  
Md. Abdul Gafur<sup>2</sup>, and Muhammad Abdullah Al Mamun<sup>1\*</sup>

<sup>1</sup>Department of Materials Science and Engineering, University of Rajshahi, Rajshahi-6205, Bangladesh

<sup>2</sup>Institute of Pilot Plant and Process Development Centre, Bangladesh Council of Scientific and Industrial Research (BCSIR), Dhaka-1205.

\*Corresponding author, Email address: [mamun\\_mse@ru.ac.bd](mailto:mamun_mse@ru.ac.bd)

Received 17 Mar 2022,  
Revised 21 July 2022,  
Accepted 23 July 2022

### Keywords

- ✓ Nanoparticles
- ✓ Nanocomposites,
- ✓ Epoxy resin,
- ✓ Nickel Ferrite,
- ✓ Superparamagnetic.

[mamun\\_mse@ru.a.bd](mailto:mamun_mse@ru.a.bd);  
Phone: +8801717548106

### Abstract

The epoxy matrix based nanocomposites were fabricated incorporating chemical co-precipitation synthesized Inorganic Nickel Ferrite (NiFe<sub>2</sub>O<sub>4</sub>) nanoparticles. Different physical, chemical, mechanical, electrical, optical and thermal properties of polymer matrix on the effect of nanoparticles was evaluated. Several functional groups were present in NiFe<sub>2</sub>O<sub>4</sub> nanoparticles, neat epoxy and NiFe<sub>2</sub>O<sub>4</sub>/epoxy nanocomposites that obtained from Fourier-Transform Infrared spectroscopy (FTIR). The NiFe<sub>2</sub>O<sub>4</sub> nanoparticles show superparamagnetic behaviour that was revealed by the Vibrating Sample Magnetometer (VSM). By incorporation of nanoparticles into the epoxy matrix decreased the tensile and flexural strength, and increased hardness of the composites. The improvement in light absorbance of NiFe<sub>2</sub>O<sub>4</sub>/epoxy nanocomposites was increased with increasing the NiFe<sub>2</sub>O<sub>4</sub> content. In addition, the optical band gap and dc resistivity were decreased with increasing nanoparticles addition.

## 1. Introduction

The present world give a great emphasis on the study and development of nano size materials like nanocomposite that exhibits excellent optical, electrical, chemical and magnetic properties [1-4]. These properties are dissimilar from their constituent materials which make them a promising candidate for scientific and technical interests [5-9]. Researchers are developing a sort of techniques to reduce the particle size of the filler materials which simultaneously increase the surface area of the filler, that is essential to transfer the load between the polymer matrix and the fillers. These nanocomposites may express a noticeable improvement on mechanical, thermal and electrical properties which are quite difficult to acquire from traditional microscale fillers, for instance, aramid, glass or carbon fibers. Nowadays electronics, automobile, aerospace, marine and other engineering industries show a great demand on these nanocomposites due to their outstanding mechanical and thermal properties. Ferrite is a special class of magnetic materials belonging from spinel group. Because of their some superior properties they can be used in microwave, transformer cores, magnetic memories, isolators, noise filters, etc. [10-13]. Nickel ferrite (NiFe<sub>2</sub>O<sub>4</sub>) is one of the most common spinel magnetic material which shows high electro-magnetic performance, excellent chemical stability and mechanical hardness, high coercivity, and moderate saturation magnetization that make it a good candidate for the

application as soft magnets and low loss materials at high frequencies [14,15]. Various methods are available for the synthesis of nanostructured ferrite nanoparticles such as- chemical vapour deposition, hydrothermal synthesis [16], sonochemical technique, chemical precipitation [17], sol-gel technique [18], microemulsion technique [19], hydrolysis [20], ball milling [21], laser ablation, sputtering, and spray pyrolysis [22].

In 2009, K. Maaz *et al.* synthesized nickel ferrite nanoparticles by co-precipitation method [23]. They produced superparamagnetic nickel ferrite with the particles size ranges between 8-28 nm. In 2012, L.S. Fu *et al.* synthesized superparamagnetic nickel ferrite colloidal spheres for constructing magnetically responsive photonic crystals [24]. They followed simple hydrothermal method to synthesize nickel ferrite colloidal spheres with tuneable compositions with superparamagnetic properties which latter used to construct photonic crystals. In 2014, Seema Joshi *et al.* studied the Structural, magnetic, dielectric and optical properties of nickel ferrite nanoparticles synthesized by co-precipitation method [25]. They produced nickel ferrite with an average particle size of 8-20 nm and found that the increase in sintering temperature increases the saturation magnetization, coercivity and remanence of nickel ferrite. In 2015, M. Khairy *et al.* studied electrical and optical properties of nickel ferrite/polyaniline nanocomposites [26]. They produced NiFe<sub>2</sub>O<sub>4</sub>/PANI nanocomposites by in-situ polymerization which can be used in supercapacitors, sensors, batteries, electrodes, etc.

On the contrary, Epoxy resin is one of the most important thermosetting polymers with some excellent properties e.g. light weight, chemically resistance, oil and fuel resistance, electrically resistance which make it a good candidate in electrical, electronics and industrial applications [27]. In 2011, Richard Voo *et al.* fabricated epoxy nanocomposite films by spin coating technique where synthetic diamond, silicon nitride and boron nitride were dispersed to enhance the tensile strength and young modulus of the epoxy resin [28]. In 2016, A. Kanapitsas *et al.* investigated that incorporation of barium ferrite into epoxy matrix decreases the relative permittivity, magnetic coercivity and absorption of water [29]. In 2016, Masoomah Gazderazi *et al.* observed that incorporation of MWCNT with nano metal oxides and TiO<sub>2</sub> greatly increases the tensile, flexural and compressive characteristics as well as the thermal conductivity of epoxy matrix [30].

Addition of nanoparticles into the polymer matrix greatly influence the mechanical and thermal properties of the nanocomposites [31-34]. Here, we present a procedure for the synthesis of NiFe<sub>2</sub>O<sub>4</sub> nanoparticles, which further used as a filler material for the epoxy resin. Nickel ferrite nanoparticles were synthesized by co-precipitation method using analytical grade ferric chloride and nickel chloride salts as precursor solution, where sodium hydroxide used as precipitating agent. Superparamagnetic nickel ferrite with various composition containing epoxy matrix nanocomposites were fabricated by hand layup method on flat glass mold. The samples were characterized by various experimental techniques, and the influence of NiFe<sub>2</sub>O<sub>4</sub> nanoparticles on the mechanical, thermal, optical and electrical properties of NiFe<sub>2</sub>O<sub>4</sub>/epoxy nanocomposites was investigated.

## 2. Materials and Methods

### 2.1 Materials

During synthesis, all the chemical reagents were analytical grade and used without further purification. Anhydrous Ferric Chloride (FeCl<sub>3</sub>), anhydrous Nickel Chloride (NiCl<sub>2</sub>) and Sodium Hydroxide (NaOH) were purchased from Merck (India) with a purity  $\geq 98\%$ , whereas Epoxy Resin and Diethylene Triamine (DETA) hardener were purchased from Sigma-Aldrich (India).

## **2.2 Synthesis of NiFe<sub>2</sub>O<sub>4</sub> Nanoparticles**

Nickel ferrite nanoparticles (NiFe<sub>2</sub>O<sub>4</sub>) were prepared by chemical co-precipitation method using 100ml 0.4M ferric chloride (FeCl<sub>3</sub>) and 100ml 0.2M nickel chloride (NiCl<sub>2</sub>) as precursor solutions. 3M solution of sodium hydroxide dropwise added to the salt solutions as a precipitating agent with continuous stirring and monitored the pH of the solution up to 12. After that, 2-3 drops of oleic acid added to the above solution as surfactant and heated the solution at 80 °C for 60 minutes with continuous stirring. The product was then cooled to room temperature and washed with distilled water for several times in order to remove unnecessary impurities and surfactants from the precipitated sample. Then the sample was dried above 80 °C over the night. Finally, the acquired products was grinded into a fine powder and then annealed at 250 °C for 4 hours.

## **2.3 Fabrication of NiFe<sub>2</sub>O<sub>4</sub>/Epoxy Nanocomposites**

In order to fabricate NiFe<sub>2</sub>O<sub>4</sub>/Epoxy nanocomposites, a desired amount of previously synthesized NiFe<sub>2</sub>O<sub>4</sub> nanoparticles was emerged into the epoxy resin and mixed carefully for 15 minutes in order to get a uniform dispersion of the nanoparticles within the resin. After that, hardener diethylene triamine (DETA) was incorporated into the above mixture and mixed properly (epoxy-curing agent ratio was 10:1 by weight). Finally, the mixture was placed into a flat glass mold and outgassed overnight. The obtained planar composite samples had an approximate thickness of 2 mm. Because of the large surface area and high aspect ratio of the nanoparticles, the content of NiFe<sub>2</sub>O<sub>4</sub> nanoparticles in the composite were chosen to be 0.5, 1.0, 2.5, and 5.0 wt% respectively. It should be noted that the mixing of the epoxy resin and the NiFe<sub>2</sub>O<sub>4</sub> nanoparticles was carried out in a controlled ambience but at the end, we could not prevent a certain particle agglomeration.

## **2.4 X-Ray Diffraction (XRD)**

XRD patterns of NiFe<sub>2</sub>O<sub>4</sub> nanoparticles were taken using a BRUKAR ADVANCE D8 Diffractometer. Bragg's angle (2θ) varying from 10° to 70° and the diffraction patterns were recorded at room temperature using Cu Kα radiation (λ = 1.5406 Å).

## **2.5 Scanning Electron Microscopy (SEM)**

The morphology of NiFe<sub>2</sub>O<sub>4</sub> nanoparticles and NiFe<sub>2</sub>O<sub>4</sub>/epoxy nanocomposites were observed using JEOLUSER 7610F Scanning Electron Microscope, which operated at 5 kV.

## **2.6 Fourier-Transform Infrared Spectroscopy (FTIR)**

To confirm the presence of different functional groups, Fourier transform Infrared (FTIR) spectra of NiFe<sub>2</sub>O<sub>4</sub> nanoparticles, neat epoxy and NiFe<sub>2</sub>O<sub>4</sub>/epoxy nanocomposites were recorded on a PERKIN-ELMER FRONTIER FTIR/MIR Spectrometer within 450-4000 cm<sup>-1</sup> region.

## **2.7 Vibrating Sample Magnetometer (VSM)**

The magnetic hysteresis curve of NiFe<sub>2</sub>O<sub>4</sub> nanoparticles were obtained from MICROSENSE EV9 Vibrating Sample Magnetometer at room temperature.

## **2.8 Tensile Strength Testing**

Tensile properties of neat epoxy and NiFe<sub>2</sub>O<sub>4</sub>/epoxy nanocomposites were measured using HOUNSFIELD H10KS UTM Machine. The length and width of the specimens were 60 mm and 10 mm, respectively. The test was performed at 2 mm/min extension speed.

## 2.9 Hardness Testing

The hardness of neat epoxy and NiFe<sub>2</sub>O<sub>4</sub>/epoxy nanocomposites were tested by SHIMADZU HMV-2 VICKER'S Micro-Hardness Tester. The specimen was placed on a hard, horizontal glass surface. The diamond indenter was held in vertical position and the scale was performed with 10 seconds, after the pressure was in the firm contact with the specimen.

## 2.10 Flexural Strength Testing

The flexural properties of neat epoxy and NiFe<sub>2</sub>O<sub>4</sub>/epoxy nanocomposites were determined using HOUNSFIELD H10KS UTM Machine. The specimens were designed as 60 mm in length, 10 mm in width and 2 mm in thickness. The span-to-depth ratio was set as 41:2 and the tests were carried out at constant cross-head speed of 2 mm/min.

## 2.11 Thermogravimetric Analysis (TGA)

The TGA curves of NiFe<sub>2</sub>O<sub>4</sub> nanoparticles, neat epoxy and NiFe<sub>2</sub>O<sub>4</sub>/epoxy nanocomposites were obtained from EXSTAR 6000, TG/DTA 6300 Thermal Analyzer with a heating rate of 20 °C/min. The mass of the solid specimen was about 2-3 mg and the whole measurements were carried out in nitrogen atmosphere.

## 2.12 UV-Vis Spectroscopy

The optical band gap of neat epoxy and NiFe<sub>2</sub>O<sub>4</sub>/epoxy nanocomposites were measured at room temperature using SHIMADZU UV-1601 Spectrophotometer within the range of 190-1100 nm.

## 2.13 DC Resistivity

The dc resistivity of neat epoxy and NiFe<sub>2</sub>O<sub>4</sub>/epoxy nanocomposites were measured using KEITHLEY 6517B Electrometer up to 50 volts at room temperature.

# 3. Results and Discussion

## 3.1 XRD Analysis

The X-ray diffraction (XRD) patterns of NiFe<sub>2</sub>O<sub>4</sub> nanoparticles are shown in [figure 1](#). This pattern is used to determine the crystal structure, and particle size of NiFe<sub>2</sub>O<sub>4</sub> nanoparticles. In the XRD patterns, the most intense XRD peak appeared at  $2\theta = 31.702^\circ$  represent the (311) plane of NiFe<sub>2</sub>O<sub>4</sub> nanoparticles (inverse spinel structure) [35]. In crystalline NiFe<sub>2</sub>O<sub>4</sub>, the considered diffraction peaks appeared at  $2\theta$  values of  $27.316^\circ$ ,  $31.702^\circ$ ,  $35.20^\circ$ ,  $45.440^\circ$ ,  $56.456^\circ$  and  $62.82^\circ$  correspond to the crystal planes (220), (311), (222), (400), (422) and (511) respectively. The crystal structure of NiFe<sub>2</sub>O<sub>4</sub> nanoparticles were indexed as inverse spinel and face centred cubic (FCC) which matched with the standard JCPDS Card No. 10-0325 [36]. Diffraction peaks of other impurities like  $\alpha$ -Fe<sub>2</sub>O<sub>3</sub>, NiO were not observed. Using Debye-Scherrer's relation [37], the crystallite size of NiFe<sub>2</sub>O<sub>4</sub> sample is calculated as follows:

$$D = \frac{K\lambda}{\beta \cos\theta}$$

Where  $\lambda$  is the wavelength of the X-ray radiation (1.5406 Å), K is a constant taken as 0.94,  $\theta$  is the diffraction angle and  $\beta$  is the full width at half maximum (FWHM) [38]. Using Instanano software, we calculated the average crystallite size of NiFe<sub>2</sub>O<sub>4</sub> nanoparticles that was about 40 nm.

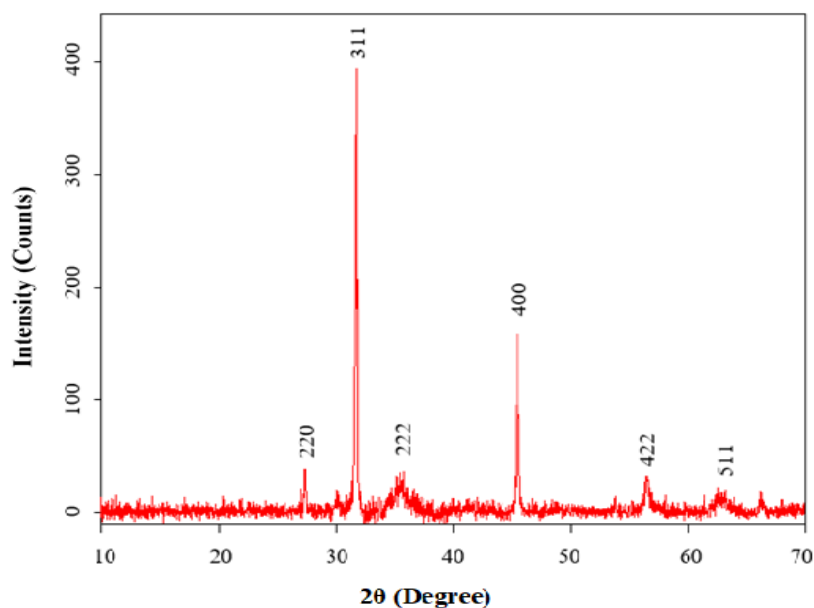


**Figure 1** XRD patterns of NiFe<sub>2</sub>O<sub>4</sub> nanoparticles.

### 3.2 SEM Analysis

The SEM images of NiFe<sub>2</sub>O<sub>4</sub> nanoparticles and NiFe<sub>2</sub>O<sub>4</sub>/epoxy nanocomposites are illustrated in figure 2(a) and (b) with  $\times 100,000$  and  $\times 5,000$  magnification, respectively. From the figure 2, it is seen that, NiFe<sub>2</sub>O<sub>4</sub> nanoparticles are well organized and looks like small spherical shaped particles. The average crystallite size of NiFe<sub>2</sub>O<sub>4</sub> nanoparticles from SEM image, which was found to be approximately 44 nm. It is obvious that NiFe<sub>2</sub>O<sub>4</sub> nanoparticles are mainly present as granules with small and big spherical shaped particles and are well crystalline in nature.

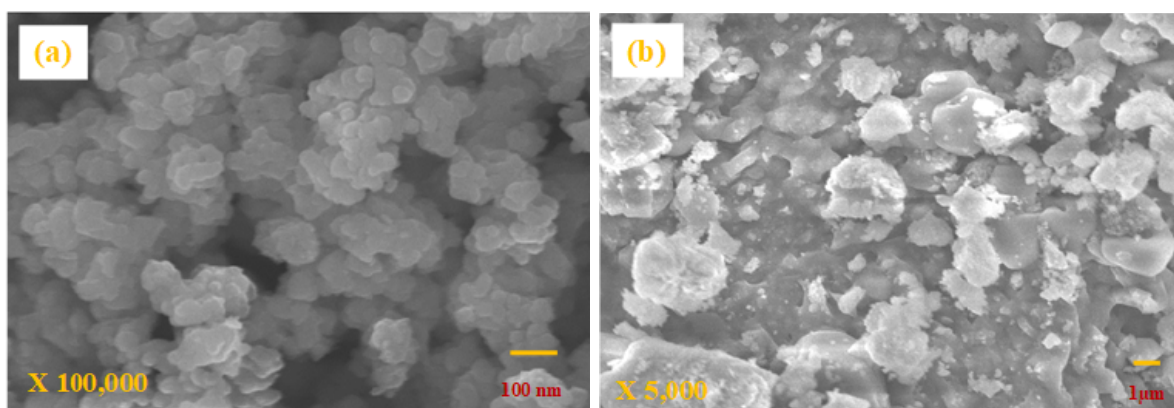


**Figure 2** SEM image of NiFe<sub>2</sub>O<sub>4</sub> nanoparticle

### 3.3 FTIR Analysis

Figure 3 shows the FTIR spectrum of NiFe<sub>2</sub>O<sub>4</sub> nanoparticles, neat epoxy and 2.5% NiFe<sub>2</sub>O<sub>4</sub>/epoxy nanocomposite. For NiFe<sub>2</sub>O<sub>4</sub> nanoparticles, the band at 3472 cm<sup>-1</sup> ascribes to the stretching mode of H-O-H bond of the free or absorbed water. The band at 541 cm<sup>-1</sup> corresponds to intrinsic stretching vibrations of the metal at the tetrahedral site (Fe  $\leftrightarrow$  O), whereas the band at 450 cm<sup>-1</sup> is assigned to octahedral metal stretching (Ni  $\leftrightarrow$  O). The difference in the absorption position in octahedral and tetrahedral complexes of NiFe<sub>2</sub>O<sub>4</sub> crystal is due the different distance between Fe<sup>3+</sup> – O<sup>2-</sup> in the octahedral and tetrahedral sites. These two strong absorption bands are of inverse spinel ferrite and the positions of these infrared bands are in the ranges which correspond to NiFe<sub>2</sub>O<sub>4</sub>.

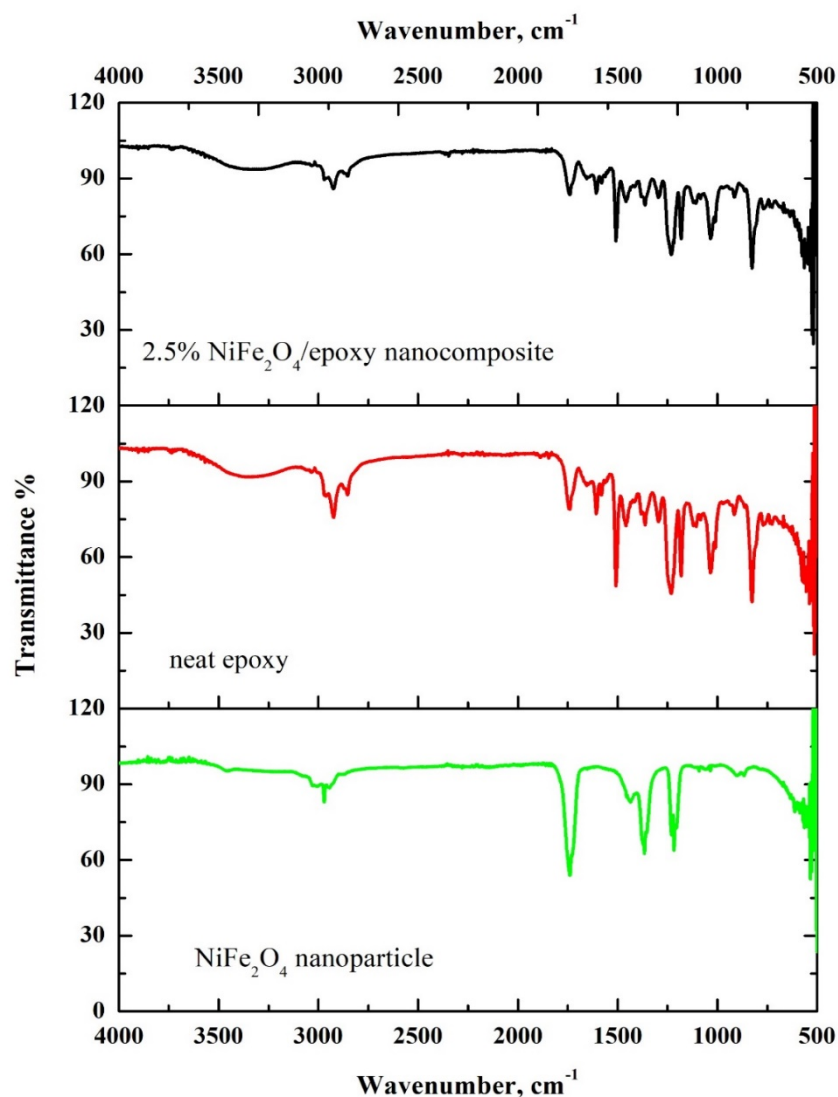


**Figure 3** FTIR spectrum of NiFe<sub>2</sub>O<sub>4</sub> nanoparticles, neat epoxy and 2.5% NiFe<sub>2</sub>O<sub>4</sub>/Epoxy nanocomposite

The peak around 1215 cm<sup>-1</sup> is due to the stretching vibrations of the anti-symmetric NO<sub>3</sub><sup>-</sup> group. There is no peak at 2900 cm<sup>-1</sup> indicating the C-H stretching band, which means all organic compounds are removed from the samples after calcinations at 250 °C. For neat epoxy, the O-H, C-H, C=O, C=C, C=N and C-O stretching vibration peaks were appeared at 3330, 2926, 1748, 1510, 1238 and 1037 cm<sup>-1</sup> respectively. The C-H bending vibration peak was found at 1366 cm<sup>-1</sup>. For 2.5% NiFe<sub>2</sub>O<sub>4</sub>/epoxy nanocomposite, the O-H, C-H, C=O, C=C, C-N and C-O stretching vibration peaks were appeared at 3371, 2917, 1742, 1508, 1233 and 1036 cm<sup>-1</sup>, respectively. The C-H bending vibration peak is appeared at 1370 cm<sup>-1</sup>.

### 3.4 VSM Analysis

A Vibrating Sample Magnetometer was operated at room temperature to measure the magnetic properties of NiFe<sub>2</sub>O<sub>4</sub> nanoparticles. The magnetization-magnetic field hysteresis curve of NiFe<sub>2</sub>O<sub>4</sub> nanoparticles is shown in [figure 4](#). Because of its nano size dimension, NiFe<sub>2</sub>O<sub>4</sub> nanoparticles exhibited superparamagnetic behavior. The saturation magnetization ( $M_s$ ), coercivity ( $H_c$ ) and remnant magnetization ( $M_r$ ) of NiFe<sub>2</sub>O<sub>4</sub> nanoparticles were  $81.058 \times 10^{-3}$  emu, 18.892 Oe and  $1.264 \times 10^{-3}$  emu, respectively. It is reported that the magnetic properties of the materials basically depend on the particles size, shape, magnetization direction, crystallinity, etc.

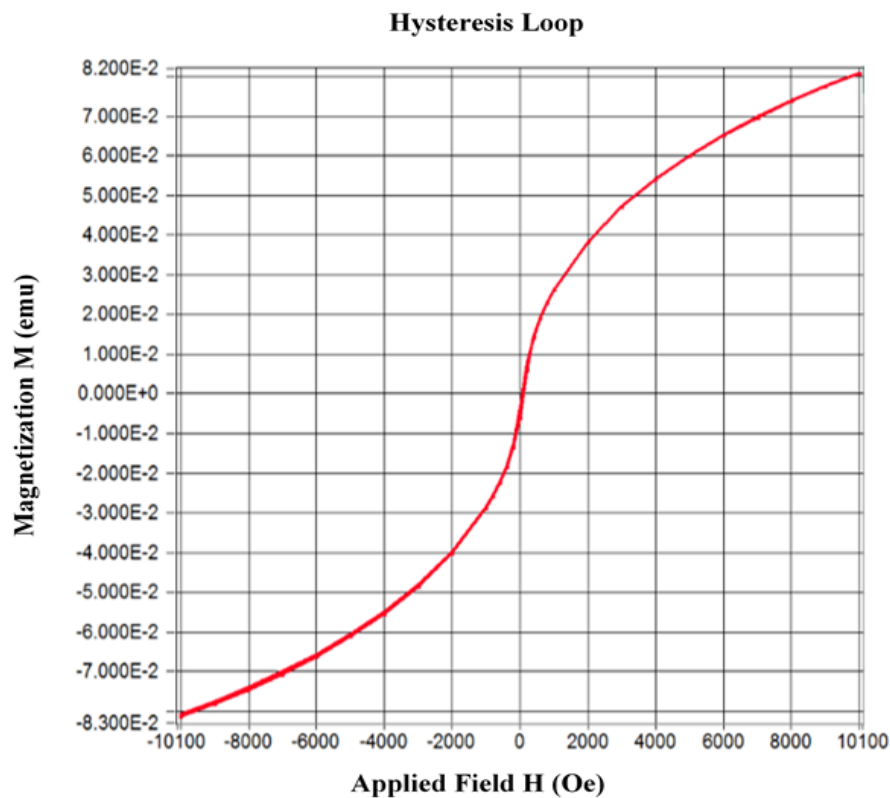


**Figure 4** Magnetization-magnetic field hysteresis curve of NiFe<sub>2</sub>O<sub>4</sub> nanoparticles.

### 3.5 Tensile Strength Analysis

Figure 5 shows the stress-strain diagram of neat epoxy, 0.5, 1.0, 2.5 and 5.0 wt% NiFe<sub>2</sub>O<sub>4</sub>/epoxy nanocomposites. Epoxy resin and NiFe<sub>2</sub>O<sub>4</sub> both are brittle materials because of their failure in tension at comparatively low values of strain. The initial linear curve in the diagram represents the elastic region, where the stress and strain are directly proportional.

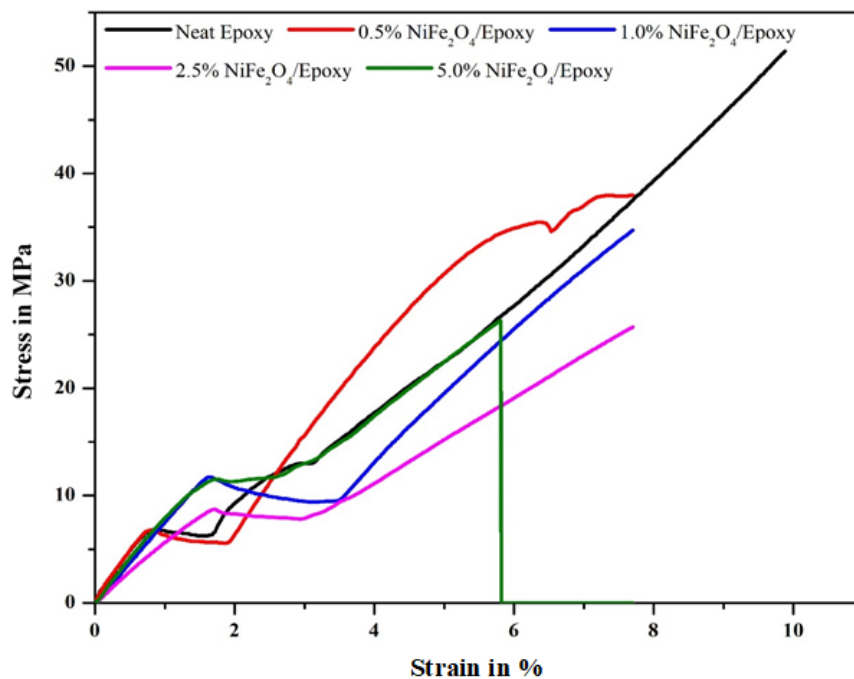


**Figure 5** Stress-strain curves of NiFe<sub>2</sub>O<sub>4</sub>/Epoxy nanocomposites.

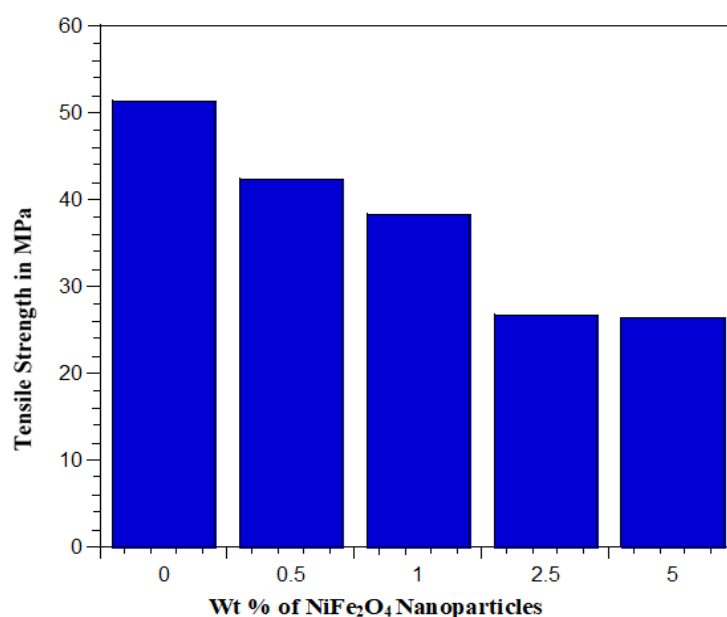
The tensile modulus of the material was measured from the slope of 0.1 to 0.25% tensile strain. The measured tensile properties of NiFe<sub>2</sub>O<sub>4</sub>/epoxy nanocomposites are illustrated in Table 1. From the table 1, it is noticed that the presence of NiFe<sub>2</sub>O<sub>4</sub> nanoparticles greatly affect the tensile stress-strain behavior of the epoxy polymer. Nanocomposites exhibited higher tensile modulus which was expected, because the modulus of NiFe<sub>2</sub>O<sub>4</sub> nanoparticles is about 220 GPa [39]. Addition of NiFe<sub>2</sub>O<sub>4</sub> nanoparticles into epoxy matrix reduced the tensile strength of the nanocomposites because epoxy resin and NiFe<sub>2</sub>O<sub>4</sub> nanoparticles both shows compressive characteristics as shown in Figure 6.

**Table 1** Tensile properties of neat epoxy and NiFe<sub>2</sub>O<sub>4</sub>/epoxy nanocomposites.

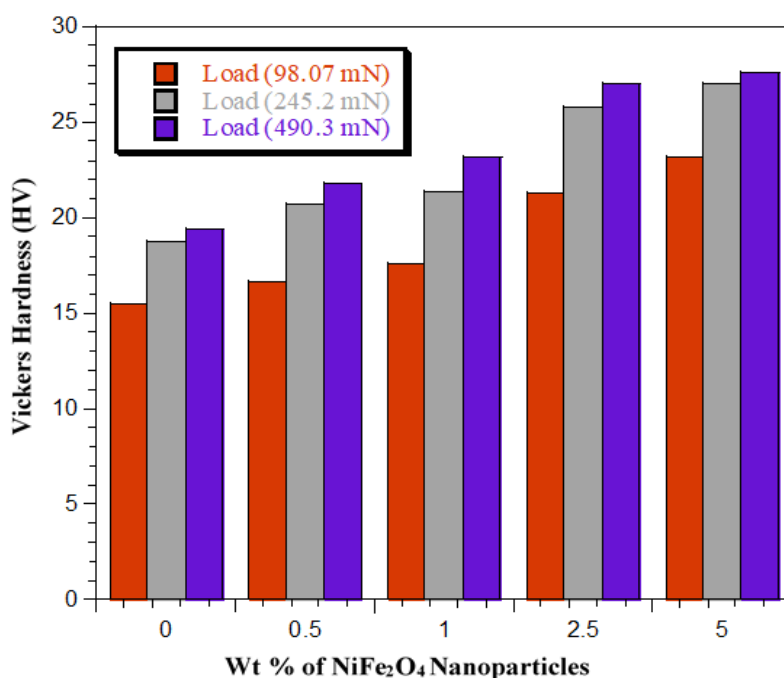
Materials	Yield Strength (MPa)	Tensile Strength (MPa)	Elongation (%)	Young Modulus (MPa)	Energy (J)
Neat Epoxy	6.88	51.40	9.880	919	0.7140
0.5% NiFe <sub>2</sub> O <sub>4</sub> /Epoxy	6.80	42.40	5.120	1694	0.5910
1.0% NiFe <sub>2</sub> O <sub>4</sub> /Epoxy	11.74	38.35	3.372	1815	0.2020
2.5% NiFe <sub>2</sub> O <sub>4</sub> /Epoxy	8.71	26.71	3.188	1406	0.1796
5.0% NiFe <sub>2</sub> O <sub>4</sub> /Epoxy	26.31	26.31	2.324	1923	0.1565

### 3.6 Hardness Analysis

Hardness is the property of a material which restrict the plastic deformation, usually by penetration, bending, scratching, abrasion or cutting. In the present work, the hardness of the neat epoxy, 0.5, 1.0, 2.5 and 5.0 wt% of NiFe<sub>2</sub>O<sub>4</sub>/epoxy nanocomposites were determined by Vickers's micro-hardness tester. The tests were carried out at three different loads 98.07, 245.2 and 490.3 mN, respectively as shown in figure 7. The Vickers hardness number significantly increased for NiFe<sub>2</sub>O<sub>4</sub>/epoxy nanocomposites compared to the pristine epoxy. This might be due to the addition of NiFe<sub>2</sub>O<sub>4</sub> nanoparticles into epoxy matrix restricted the movement of dislocation within the structure of epoxy matrix, consequently increased the hardness number.



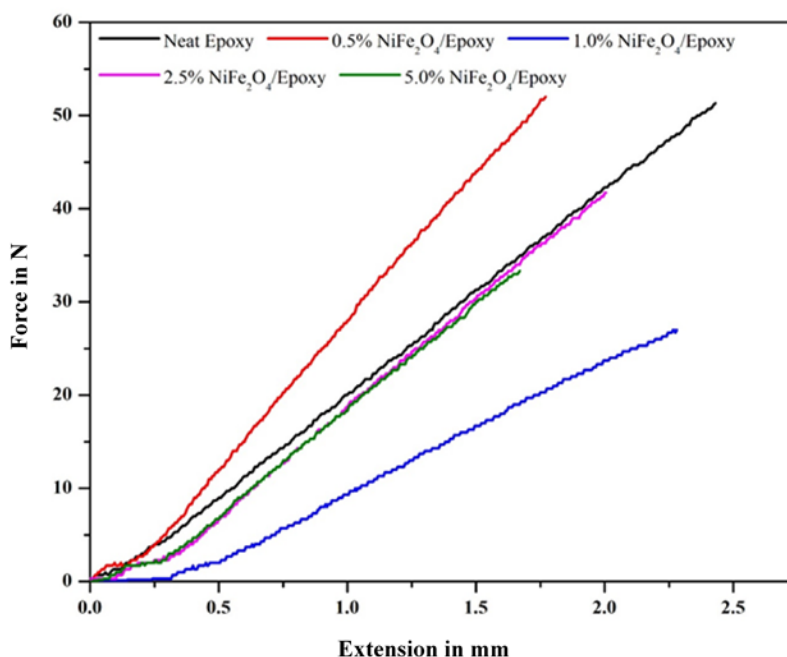
**Figure 6** Effect of NiFe<sub>2</sub>O<sub>4</sub> nanoparticles on the tensile strength of NiFe<sub>2</sub>O<sub>4</sub>/Epoxy nanocomposites.



**Figure 7** Effect of NiFe<sub>2</sub>O<sub>4</sub> nanoparticles on the hardness of NiFe<sub>2</sub>O<sub>4</sub>/Epoxy nanocomposites

### 3.7 Flexural Strength Analysis

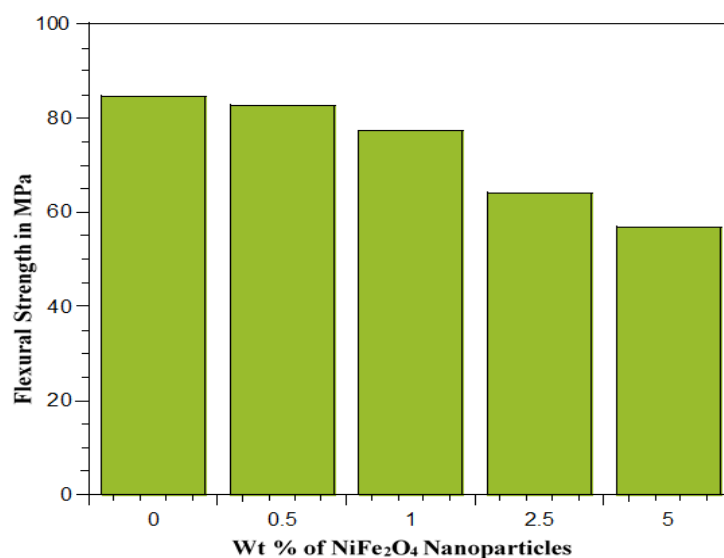
The three-point flexural test was performed to measure the flexural properties of nanocomposites with/without the addition of NiFe<sub>2</sub>O<sub>4</sub> nanoparticles into the epoxy matrix, whose force-extension curves are given in figure 8. The neat epoxy, 0.5, 1.0, 2.5 and 5.0 wt% of NiFe<sub>2</sub>O<sub>4</sub>/epoxy nanocomposites showed 84.5, 82.8, 77.2, 64.1 and 56.9 MPa flexural strength with 1.735, 2.002, 2.441, 2.29 and 1.907% strain at break, respectively which is represented in table 2. Because of the compressive characteristics of epoxy resin and NiFe<sub>2</sub>O<sub>4</sub> nanoparticles, the incorporation of NiFe<sub>2</sub>O<sub>4</sub> nanoparticles into the epoxy matrix gradually decreased the flexural strength of matrix materials as shown in figure 9. Addition of filler material is not effective to improve flexural characteristics of matrix but it may increase in case of laminates with filler matrix [40].



**Figure 8** Force-extension curves of NiFe<sub>2</sub>O<sub>4</sub>/Epoxy nanocomposites.

**Table 2** Flexural properties of neat epoxy and NiFe<sub>2</sub>O<sub>4</sub>/epoxy nanocomposites.

Materials	Flexural Strength (MPa)	Strain at Break (%)	Energy (J)
Neat Epoxy	84.50	1.735	0.0601
0.5% NiFe <sub>2</sub> O <sub>4</sub> /Epoxy	82.80	2.022	0.0696
1.0% NiFe <sub>2</sub> O <sub>4</sub> /Epoxy	77.20	2.425	0.0536
2.5% NiFe <sub>2</sub> O <sub>4</sub> /Epoxy	64.10	2.290	0.0609
5.0% NiFe <sub>2</sub> O <sub>4</sub> /Epoxy	56.90	1.907	0.0400

**Figure 9** Effect of NiFe<sub>2</sub>O<sub>4</sub> nanoparticles on the flexural strength of NiFe<sub>2</sub>O<sub>4</sub>/Epoxy nanocomposite.

### 3.8 TG Analysis

**Figure 10** illustrates the TGA curves of NiFe<sub>2</sub>O<sub>4</sub> nanoparticles, neat epoxy and 5.0% NiFe<sub>2</sub>O<sub>4</sub>/epoxy nanocomposite. The decomposition process was classified into three regions, they were 20-300 °C, 300-500 °C and 500-600 °C. Because of the initial degradation of complex and spontaneous combustion, the first weight loss indicates the evaporation of absorbed water. Liberation of H<sub>2</sub>O, CO<sub>2</sub> and the nitrate ions render an oxidizing environment for the combustion of the organic compounds [41]. The second weight loss ascribes to the dehydration of O-H group in the spinel structure of some components such as NO<sub>3</sub><sup>-</sup> and epoxy that lead to two degradation systems involving both inter and intra-molecular transfer reaction, the oxidation of complexes and formation of semi-organic carbon metal/metal oxide [42-44]. The third weight loss confirms the formation of corresponding metal oxide and the spinel phase. There was no weight loss above 600 °C, i.e. TGA curves were steady which indicates the absolute volatility of water, organic compound, nitrates in the composites, the completion of crystallization route and the immediate formation of pure materials.

### 3.9 UV-Vis Spectroscopy Analysis

UV-Vis spectra of NiFe<sub>2</sub>O<sub>4</sub>/epoxy nanocomposites were performed within 190-1100 nm range, which is used to determine the optical band gap of the nanocomposites as shown in **figure 11**. The spectrum of epoxy showed a single absorption peak at 526 nm, which is attributed to polaron/bipolaron transition. While the spectra of NiFe<sub>2</sub>O<sub>4</sub>/epoxy nanocomposites showed several peaks, appeared between the entire wavelength in shells, raised the absorption cross section of the nanocomposites and thus influence the plasma-exciton interactions [45-47]. The following equation was used to determine the optical band gap energy [48]:

$$(\alpha h\nu)^{1/n} = A (h\nu - E_g)$$

For direct band gap materials this equation becomes-

$$(\alpha h\nu) = A (h\nu - E_g)^2$$

where  $\alpha$  represents the absorption coefficient,  $A$  is a constant,  $E_g$  indicates the optical band gap of the material and the exponent  $n$  depends on the nature of electronic transition, it is equal to 1/2 for direct allowed, 3/2 for direct forbidden transitions and 2 for indirect allowed transition.

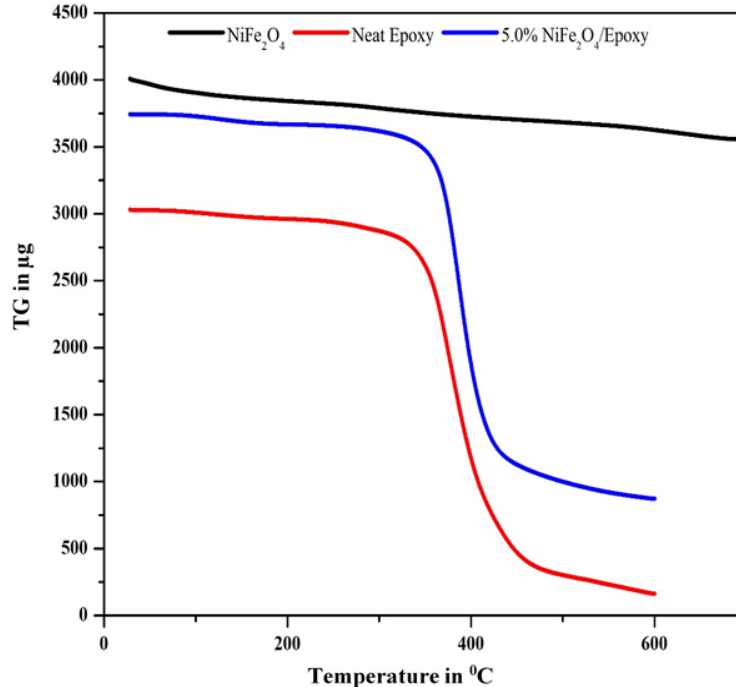


**Figure 10** TGA curves of NiFe<sub>2</sub>O<sub>4</sub> nanoparticles, neat epoxy and 5.0% NiFe<sub>2</sub>O<sub>4</sub>/Epoxy nanocomposit

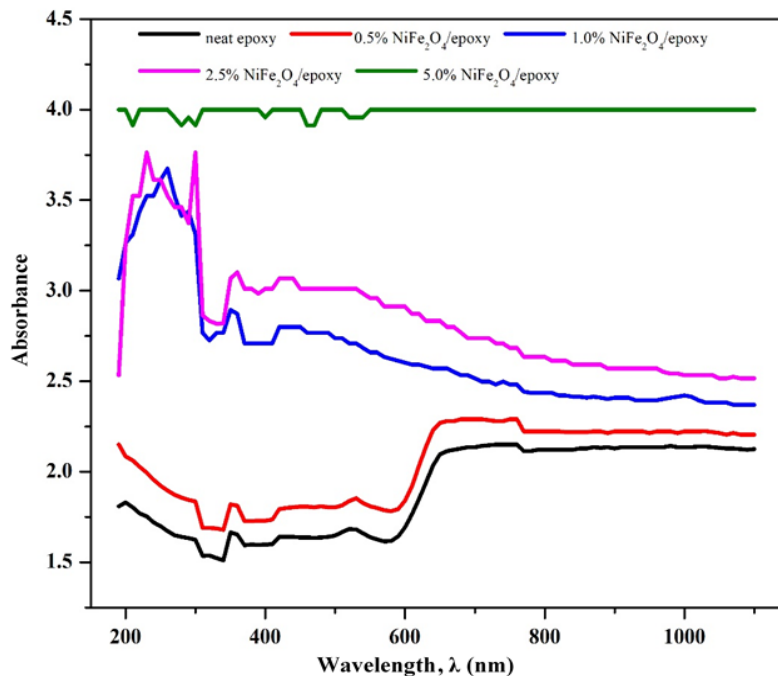


**Figure 11** Absorbance vs wavelength curves of NiFe<sub>2</sub>O<sub>4</sub>/Epoxy nanocomposites.

An extrapolation of the linear region of a plot of the graph of  $(\alpha h\nu)^2$  on the y-axis versus photon energy  $(h\nu)$  on the x-axis, gives the value of the optical band gap,  $E_g$  [49] which is illustrated in the figure 12. From the figure 11 it is seen that, incorporation of NiFe<sub>2</sub>O<sub>4</sub> nanoparticles increased the absorbance of

NiFe<sub>2</sub>O<sub>4</sub>/epoxy nanocomposites. In contrast, [figure 12](#) represents the measured optical band gap of neat epoxy, 0.5, 1.0, 2.5 and 5.0 wt% of NiFe<sub>2</sub>O<sub>4</sub>/epoxy nanocomposites which was 3.2, 3.2, 2.6, 2.3 and 1.8 eV, respectively.

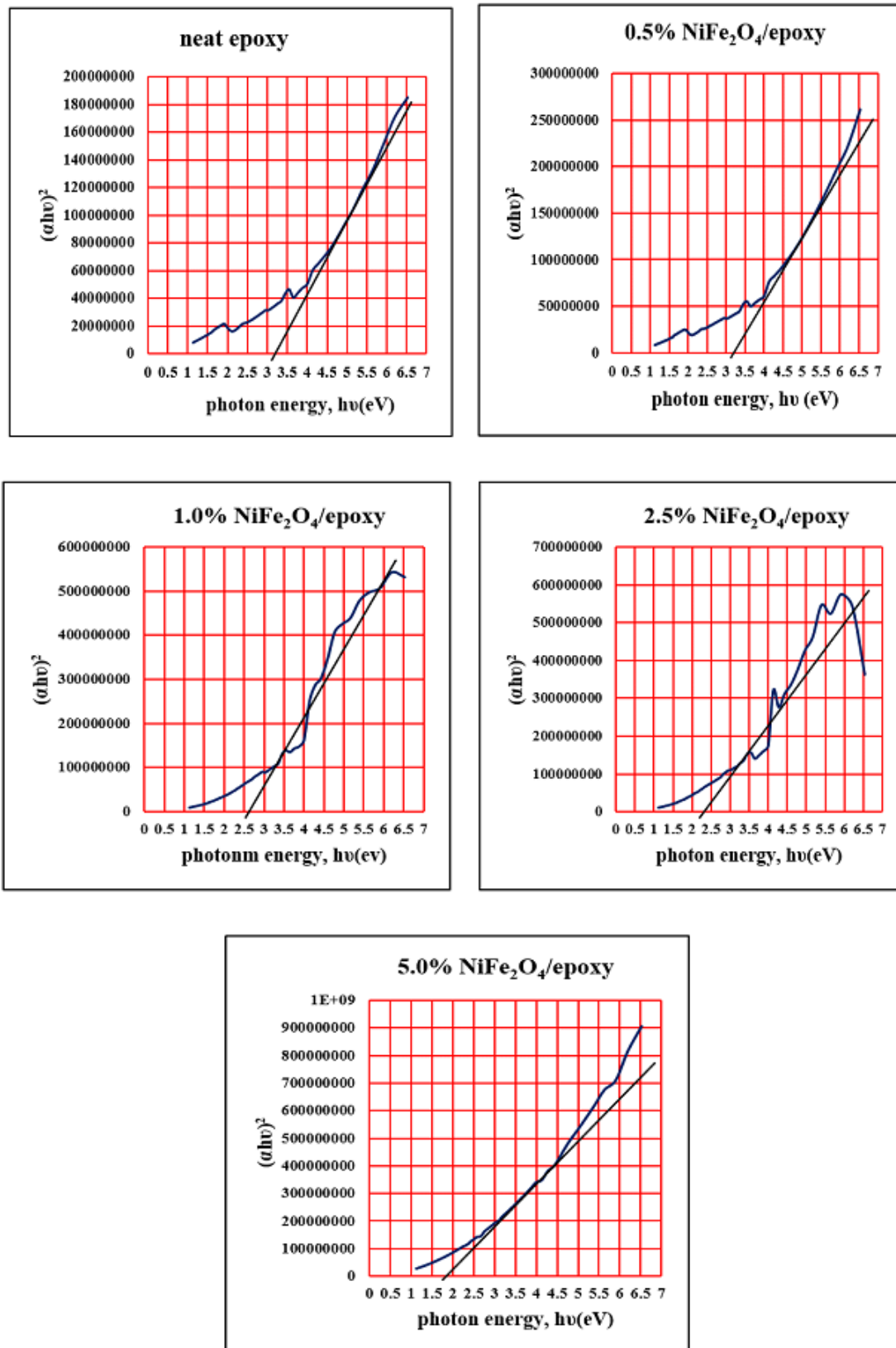


**Figure 12** Optical band gap of NiFe<sub>2</sub>O<sub>4</sub>/Epoxy nanocomposites.

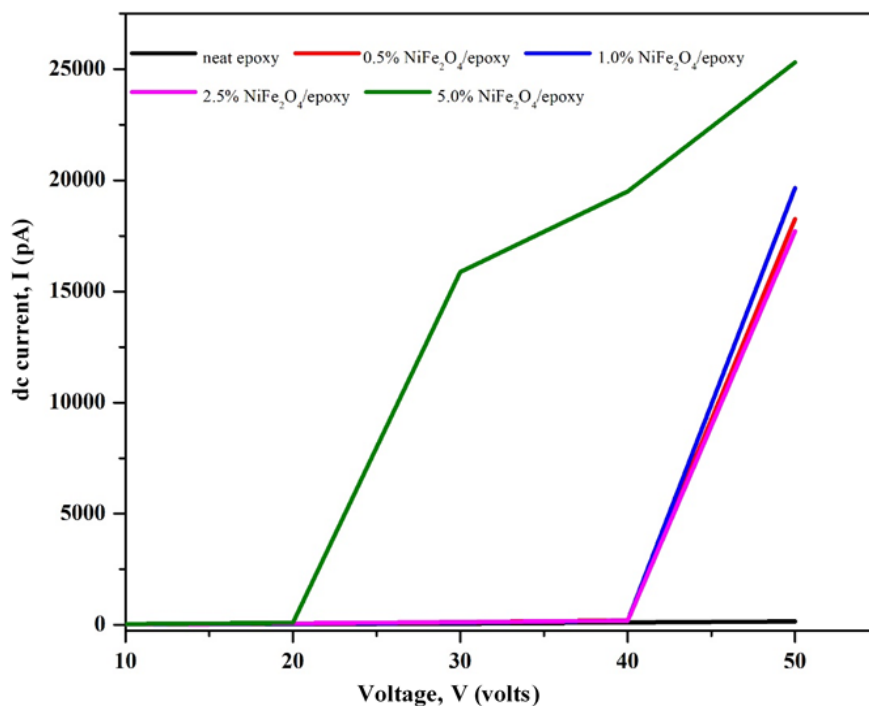


**Figure 13** I-V curves of NiFe<sub>2</sub>O<sub>4</sub>/Epoxy nanocomposites.

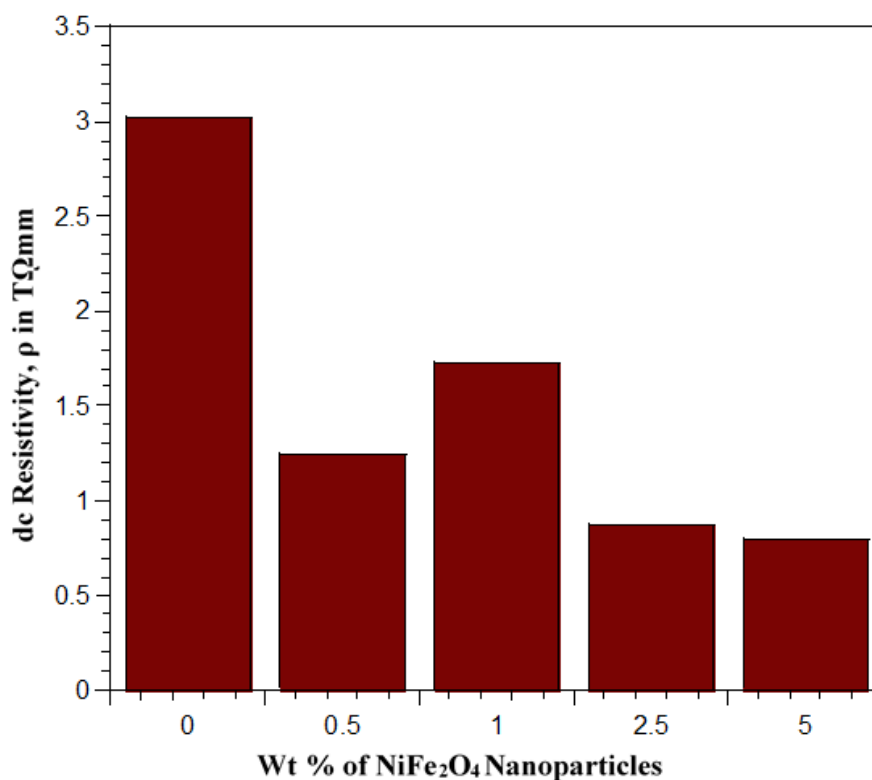


**Figure 14** Effect of NiFe<sub>2</sub>O<sub>4</sub> nanoparticles on the dc resistivity of NiFe<sub>2</sub>O<sub>4</sub>/Epoxy nanocomposites.

### 3.10 DC Resistivity Analysis

Figure 13 illustrates the I-V curves of neat epoxy, 0.5, 1.0, 2.5 and 5.0 wt% of NiFe<sub>2</sub>O<sub>4</sub>/epoxy nanocomposites, where all the tests were carried out at room temperature. From this figure it is seen that, 5.0 % NiFe<sub>2</sub>O<sub>4</sub>/epoxy nanocomposite showed the higher value of dc current, I (about 25.312 nA) at 50

volts, while neat epoxy exhibited the minimum value of dc current,  $I$  (about 18.741 A) at 10 volts. Conversely, [figure 1](#) demonstrates that neat epoxy exhibited the highest value of dc resistivity,  $\rho$  (about 3.017 T $\Omega$ mm) due to its excellent dielectric properties, while 5.0% NiFe<sub>2</sub>O<sub>4</sub>/epoxy nanocomposite showed the lowest value of dc resistivity,  $\rho$  (about 0.793 T $\Omega$ mm). Incorporation of NiFe<sub>2</sub>O<sub>4</sub> nanoarticles into epoxy matrix reduced the dc resistivity of the nanocomposite due to the formation of polarons in the both epoxy and NiFe<sub>2</sub>O<sub>4</sub> molecules after applying voltage [50]. Somehow, 1.0% NiFe<sub>2</sub>O<sub>4</sub>/epoxy nanocomposite showed a little inconsistency in dc resistivity, this might be for non-uniform dispersion and agglomeration of certain NiFe<sub>2</sub>O<sub>4</sub> nanoarticles into the epoxy matrix.

#### 4. Conclusions

Nickel ferrite nanoparticles successfully synthesized by co-precipitation method which further added to the epoxy matrix to fabricate NiFe<sub>2</sub>O<sub>4</sub>/epoxy nanocomposites. The chemical, mechanical, electrical, optical and thermal properties of the fabricated polymer nanocomposites were evaluated. The XRD and SEM confirmed the formation of nanoparticles. FTIR analysis ensured the presence of different functional groups into the nanomaterials. VSM measurement revealed that the saturation magnetization ( $M_s$ ), coercivity ( $H_c$ ) and remnant magnetization ( $M_r$ ) of NiFe<sub>2</sub>O<sub>4</sub> nanoparticles were  $81.058 \times 10^{-3}$  emu, 18.892 Oe and  $1.264 \times 10^{-3}$  emu, respectively. A sort of properties for instance, Tensile strength, Elongation, Breaking Energy, Flexural strength, Optical band gap energy and dc resistivity of NiFe<sub>2</sub>O<sub>4</sub>/epoxy nanocomposites gradually decreased due to the incorporation of NiFe<sub>2</sub>O<sub>4</sub> nanoparticles into epoxy matrix, but it increased the Young modulus, Surface hardness and thermal stability of NiFe<sub>2</sub>O<sub>4</sub>/epoxy nanocomposites.

**Acknowledgements-** One of the authors Md. Abdus Sabur is thankful to the Ministry of Science and Information & Communication Technology (MOSICT) of People's Republic of Bangladesh for providing financial support.

#### References

- [1] M. Dariel, L.H. Bennett, D.S. Lashmore, P. Lubitz, M. Rubinstein, W.L. Lechter, M.Z. Harford, Properties of electrodeposited Co-Cu multilayer structures, *J. Appl. Phys.*, 61 (1987) 4067, <https://doi.org/10.1063/1.338529>
- [2] W.D. Williams, N. Giordano, Experimental study of localization and electron-electron interaction effects in thin Au wires, *Phys. Rev. B*, 33 (1986) 8146, <https://doi.org/10.1103/PhysRevB.33.8146>
- [3] T.M. Whitney, J.S. Jiang, P.C. Searson, C.L. Chien, Fabrication and magnetic properties of arrays of metallic nanowires, *Science*, 261 (1993) 1316, <https://doi.org/10.1126/science.261.5126.1316>
- [4] L. Piraux, J.M. George, J.F. Despres, C. Leroy, E. Ferain, R. Legras, K. Ounadjela, A. Fert, Giant magnetoresistance in magnetic multilayered nanowires, *Appl. Phys. Lett.*, 65 (1994) 2484, <https://doi.org/10.1063/1.112672>
- [5] C. J. Brumlik, C. R. Martin, *Anal. Chem.*, 59 (1992) 2625.
- [6] Z. Cai, C. R. Martin, Electronically conductive polymer fibers with mesoscopic diameters show enhanced electronic conductivities, *J. Am. Chem. Soc.*, 111 (1989) 4138, <https://doi.org/10.1021/ja00193a077>
- [7] S.K. Chakarvarti, J. Vetter, Morphology of etched pores and microstructures fabricated from nuclear track filters, *Nucl. Instruments Methods. B*, 62 (1991) 109, [https://doi.org/10.1016/0168-583X\(91\)95936-8](https://doi.org/10.1016/0168-583X(91)95936-8)
- [8] S. K. Chakarvarti, J. Vetter, Microfabrication of metal-semiconductor heterostructures and tubules using nuclear track filters, *J. Microm. Microeng.*, 3, (1993) 57.

- [9] S. K. Chakarvarti, J. Vetter, Template synthesis—a membrane based technology for generation of nano-/micro materials: a review, *Radiat. Measur.*, 29(2) (1998) 149.
- [10] M. Hashim, Alimudin, S. Kumar, S.E. Shirsath, E. M. Mohamed, H. Chung, et al., Studies on the activation energy from the ac conductivity measurements of rubber ferrite composites containing manganese zinc ferrite, *Physica B*, 407(21) (2012) 4097-103, <https://doi.org/10.1016/j.physb.2012.06.006>
- [11] Goldman A. Modern ferrite technology. 2nd ed. New York: *Springer*, (2006).
- [12] S. E. Shirsath, R. H Kadam., S. M. Patange, M. L. Mane, A. Ghasemi, A. Morisako, Enhanced magnetic properties of Dy<sup>3+</sup> substituted Ni–Cu–Zn ferrite nanoparticles, *Appl Phys Lett*, 100 (2012) 042407-10, <https://doi.org/10.1063/1.3679688>
- [13] A. Narayanaswamy, N. Sivakumar, Influence of mechanical milling and thermal annealing on electrical and magnetic properties of nanostructured Ni–Zn and cobalt ferrites, *Bull Mater Sci*, 31, (2008) 373-80.
- [14] H.M. Fan, J.B. Yi, Y. Yang, K.W. Kho, H.R. Tan, Z.X. Shen, et al., Single-crystalline MFe<sub>2</sub>O<sub>4</sub> nanotubes/nanorings synthesized by thermal transformation process for biological applications, *ACS Nano*, 3(9) (2009) 2798-2808, <https://doi.org/10.1021/nn9006797>
- [15] M.G. Naseri, E.B. Saion, H.A. Ahangar, M. Hashim, A.H. Shaari, Simple preparation and characterization of nickel ferrite nanocrystals by a thermal treatment method, *Powder Technol.*, 212 (2011) 80-88, <https://doi.org/10.1016/j.powtec.2011.04.033>
- [16] C.Q. Hu, Z.H. Gao, X.R. Yang, Facile synthesis of single crystalline  $\alpha$ -Fe<sub>2</sub>O<sub>3</sub> ellipsoidal nanoparticles and its catalytic performance for removal of carbon monoxide, *Mater. Chem. Phys.*, 104 (2007) 429-433, <https://doi.org/10.1016/j.matchemphys.2007.03.040>
- [17] H. Asnaashari Eivari, A. Rahdar, Some properties of iron oxide nanoparticles synthesized in different conditions, *World Appl. Program.*, 3 (2013) 52-55.
- [18] D.K. Bandgar, S.T. Navale, G.D. Khuspe, S.A. Pawar, R.N. Mulik, V.B. Patil, Novel route for fabrication of nanostructured  $\alpha$ -Fe<sub>2</sub>O<sub>3</sub> gas sensor, *Mater. Sci. Semicond. Process*, 17 (2014) 67-73, <https://doi.org/10.1016/j.mssp.2013.08.016>
- [19] R. Ramesh, K. Ashok, G.M. Bhalero, S. Ponnusamy, C. Muthamizhchelvan, Synthesis and properties of  $\alpha$ -Fe<sub>2</sub>O<sub>3</sub> nanorods, *Cryst. Res. Technol.*, 45 (2010) 965-968, <https://doi.org/10.1002/crat.201000140>
- [20] H. Yan, X. Su, C. Yang, J. Wang, C. Niu, Improved photocatalytic and gas sensing properties of  $\alpha$ -Fe<sub>2</sub>O<sub>3</sub> nanoparticles derived from  $\beta$ -FeOOH nano spindles, *Ceram. Int.*, 40 (2014) 1729-1733, <https://doi.org/10.1016/j.ceramint.2013.07.070>
- [21] M.H. Mahmoud, H.H. Hamdeh, J.C. Ho, M.J. O'Shea, J.C. Walker, Mössbauer studies of manganese ferrite fine particles processed by ball milling, *J. Magn. Magn. Mater.*, 220 (2000) 139-146, [https://doi.org/10.1016/S0304-8853\(00\)00484-4](https://doi.org/10.1016/S0304-8853(00)00484-4)
- [22] S.S. Shinde, A.V. Moholkar, J.H. Kim, K.Y. Rajpure, Structural, morphological, luminescent and electronic properties of sprayed aluminium incorporated iron oxide thin films, *Surface Coatings Technol.*, 205 (2011) 3567-3577, <https://doi.org/10.1016/j.surfcoat.2010.12.022>
- [23] K. Maaz, S.Karim, A.Mumtaz, S.K.Hasanain, J.Liu, J.L.Duan, Synthesis and magnetic characterization of nickel ferrite nanoparticles prepared by co-precipitation route, *Journal of Magnetism and Magnetic Materials*, 321 (2009) 1838-1842., <https://doi.org/10.1016/j.jmmm.2008.11.098>

- [24] L.S. Fu, C.Y. Xu, W.S. Wang, J.T. Jiang, L. Zhen, Superparamagnetic nickel ferrite colloidal spheres for constructing magnetically responsive photonic crystals, *Materials Letters*, 81 (2012) 62-64, <https://doi.org/10.1016/j.matlet.2012.04.139>
- [25] Seema Joshi, Manoj Kumar, Sandeep Chhoker, Geetika Srivastava, Mukesh Jewariy, V.N. Singh, Structural, magnetic, dielectric and optical properties of nickel ferrite nanoparticles synthesized by co-precipitation method, *Journal of Molecular Structure*, 1076 (2014) 55-62, <https://doi.org/10.1016/j.molstruc.2014.07.048>
- [26] M. Khairy, M.E. Gouda, Electrical and optical properties of nickel ferrite/polyaniline nanocomposite, *Journal of Advanced Research*, 6 (2015) 555-562, <https://doi.org/10.1016/j.jare.2014.01.009>
- [27] Chunyi T and Weiqu L., Preparation of dual-curable polysiloxane and the properties of its cured films with epoxy resin, *J Plast Film Sheeting*, 26 (2010) 241-257, <https://doi.org/10.1177/8756087910387241>
- [28] Richard Voo, M Mariatti and LC Sim, Properties of epoxy nanocomposite thin films prepared by spin coating technique, *Journal of Plastic Film & Sheeting*, 27(4) (2011) 331-346, <https://doi.org/10.1177/8756087911419745>
- [29] A. Kanapitsas, C. Tsonos, G. C. Psarras, S. Kriptomou, Barium ferrite/epoxy resin nanocomposite system: Fabrication, dielectric, magnetic and hydration studies, *eXPRESS Polymer Letters*, 10(3) (2016) 227-236, <https://doi.org/10.3144/expresspolymlett.2016.21>
- [30] Masoomeh Gazderazi, Masoud Jamshidi, Hybridizing MWCNT with nano metal oxides and TiO<sub>2</sub> in epoxy composites: Influence on mechanical and thermal performances, *Journal of Applied Polymer Science*, (2016). <https://doi.org/10.1002/app.43834>
- [31] A. P. Kumar, D. Depana, N. S. Tomer, R. P. Singh, Nanoscale particles for polymer degradation and stabilization-Trends and future perspectives, *Prog. Polym. Sci.*, 34 (2009) 479.
- [32] Katsoulis, C. Kandare, E. Kandola, B. K., The effect of nanoparticles on structural morphology, thermal and flammability properties of two epoxy resins with different functionalities, *Polym. Degrad. Stabil.*, 96 (2011) 529, <https://doi.org/10.1016/j.polymdegradstab.2011.01.002>
- [33] M. K. Hossain, M. M. R. Chowdhury, M. B. Salam, J. Malone, M. V. Hosur, S. Jeelani, N. W. Bolden, Improved thermomechanical properties of carbon fiber reinforced epoxy composite using amino functionalized XDCNT, *J. Appl. Polym. Sci.*, 131(17) (2014) 40709, <https://doi.org/10.1002/app.40709>
- [34] S. Mohammadzadehmoghadam, Y. Dong, I. J. Davies, Recent progress in electrospun nanofibers: Reinforcement effect and mechanical performance, *J. Polym. Sci. part B: Polym. Phys.*, 53 (2015) 1171-1212, <https://doi.org/10.1002/polb.23762>
- [35] R. Goswami, R.L. Holtz, M.W. Rupich, G. Spanos, Formation of nanoparticles and defects in YBa<sub>2</sub>Cu<sub>3</sub>O<sub>7-δ</sub> prepared by the metal organic deposition process, *Scripta Mater*, 56 (2007) 797-800, <https://doi.org/10.1016/j.scriptamat.2007.07.014>
- [36] S. Qu, J. Wang, J.L. Kong, P.Y. Yang, G. Chen, Magnetic loading of carbon nanotube/nano-Fe<sub>3</sub>O<sub>4</sub> composite for electrochemical sensing, *Talanta*, 71 (2007) 1096-1102, <https://doi.org/10.1016/j.talanta.2006.06.003>
- [37] C. Hammond, The Basics of Crystallography and Diffraction, *Oxford University Press, Oxford*, (1997).
- [38] B.D. Cullity, S.R. Stock, Elements of X-ray Diffraction, third ed, *Prentice-Hall, Englewood Cliffs, NJ*, (2001).

- [39] D. Chicot, J. Mendoza, A. Zaoui, G. Louis, V. Lepingle, F. Roudet, J. Lesage, Mechanical properties of magnetite, hematite and goethite by instrumented indentation and molecular dynamics analysis, *Mat. Chem. Phys.*, 129(3) (2011) 862-870, <https://doi.org/10.1016/j.matchemphys.2011.05.056>
- [40] S. S. Sankari, N. Murugan, S. Sivaraj, Effect of filler materials on the mechanical and thermal properties of epoxy resin, *App. Mech. Mat.*, 206-10 (2014) 592-594, <https://doi.org/10.4028/www.scientific.net/AMM.592-594.206>
- [41] L. Guo, X. Shen, X. Meng, Y. Feng, *J. Alloys Compd.*, Effect of  $\text{Sm}^{3+}$  ions doping on structure and magnetic properties of nanocrystalline  $\text{NiFe}_2\text{O}_4$  fibers, 490 (2010) 301-306, <https://doi.org/10.1016/j.jallcom.2009.09.182>
- [42] Z. Wang, X. Liu, M. Lv, P. Chai, Y. Liu, J. Meng, *J. Phys. Chem. B*, Preparation of One-Dimensional  $\text{CoFe}_2\text{O}_4$  Nanostructures and Their Magnetic Properties, 112, (2008) 11292-11297, <https://doi.org/10.1021/jp802614v>
- [43] P. Sivakumar, R. Ramesh, A. Ramanand, S. Ponnusamy, C. Muthamizhchelvan, Synthesis and characterization of  $\text{NiFe}_2\text{O}_4$  nanosheet via polymer assisted co-precipitation method, *Mater. Lett.*, 65 (2011) 483-485, <https://doi.org/10.1016/j.matlet.2010.10.056>
- [44] Zhang, C.Y., Shen, X.Q., Zhou, J.X., Jing, M.X. and Cao, K., Preparation of spinel ferrite  $\text{NiFe}_2\text{O}_4$  fibres by organic gel-thermal decomposition process, *J. Sol-gel Sci. and Tech.*, 42(1) (2007) 95-100, <https://doi.org/10.1007/s10971-006-1515-5>
- [45] B. P. Rand and S. R. Forrest, Long range absorption enhancement in organic tandem thin film solar cells containing silver nanoclusters, *J Appl Phys*, 96 (2004) 7519-26, <https://doi.org/10.1063/1.1812589>
- [46] D. M. Schaadt, B. Feng, E. T. Yu, Enhanced semiconductor optical absorption via surface plasmon excitation in metal nanoparticles, *Appl Phys Lett*, 86 (2005) 063106, <https://doi.org/10.1063/1.1855423>
- [47] A. J. Mostafa, K. L. Rowlen, T. H. Reilly, M. J. Romero, V. D. Legamaat, Plasmon-enhanced solar energy conversion in organic bulk heterojunction photovoltaics, *Appl Phys Lett*, 92 (2008) 139901, <https://doi.org/10.1063/1.2823578>
- [48] M. Jestl, I. Maran, A. Kock, W. Beinsting, E. Gornik, Polarization sensitive surface plasmon Schotky detectors, *Opt Lett*, 14 (1989) 719-21.
- [49] A. A. Ogwu, T. Darma, and E. Bouquerel, Electrical resistivity of copper oxide thin films prepared by reactive magnetron sputtering, *J. Achie. in Mat. and Manuf. Eng.*, 24 (2007) 172-177.
- [50] M. Khairy, M. E. Gouda, Electrical and optical properties of nickel ferrite/polyaniline nanocomposite, *J. Adv. Res.*, 6(4) (2014) 555-562, <https://doi.org/10.1016/j.jare.2014.01.009>

(2022) ; <http://www.jmaterenvironsci.com>